Materials for life sciences

Check for
updates

An experimental and numerical study of sutural composites with shear stiffening gel core

Xiwen Fan[1], Shuai Liu[1], Bochao Wang[1], Yu Wang[1,*], Sheng Wang[1], and Xinglong Gong[1,*]

[1] *CAS Key Laboratory of Mechanical Behavior and Design of Materials, Department of Modern Mechanics, University of Science and Technology of China (USTC), Hefei 230027, China*

ABSTRACT

Biomimetic composites have attracted much attention because they can provide effective approaches to achieve high toughness and stiffness with limited raw materials. Smart materials and sophisticated structures are the key factors to influence the mechanical behavior of biomimetic composites. In this work, a novel biomimetic composite was developed by introducing shear stiffening gel (SSG) into sutural structures with different geometry parameters. Low-velocity impact tests with fixed boundary and free boundary were conducted. Experimental results indicated that sutural interface could effectively improve the contact stiffness and the capacity to dissipate impact energy. The force transmissibility was also reduced significantly. Meanwhile, smaller tooth angles could lead to more remarkable rate-dependent behavior of the composites. Our study pointed out that incorporating the geometry futures of sutural composites such as the tooth angles and the thickness of SSG could improve the dynamic mechanical behavior of the composites, which could provide fundamental insights into the engineering application of sutural structure.

Introduction

Sophisticated microstructures in biology materials, such as layered structures [1, 2], helical structures [3, 4], gradient structures [5, 6], are developed to implement complicated mechanical and physiological functions. They provide excellent strategies to achieve different targets for high stiffness, toughness or damping factors. Among these geometry solutions, sutural interface structures have attracted much attention due to its widespread existence from micro- to macro-scales [7–10]. Generally, the sutural composites can be considered as a kind of staggered composites with a modified interface geometry. They are composed of rigid facesheets with sutural waviness and soft interfacial enhancement materials. Their mechanical behavior can be easily designed by

modifying the geometry parameters of the sutural interface and the interfacial materials. Various theoretical models and numerical simulations have been brought out to study the constitutive mechanical properties and failure behavior [11]. Furthermore, based on 3D-printing technology, researchers fabricate these bionic composites and conduct various mechanical tests to demonstrate analytical results [12–15].

The shape of sutural geometry plays important role in the mechanical behavior of the structures. The inclined plane changes the propagation mechanism of stress [16, 17]. Shear stress comes to be more important in the sutural composites. Changes of geometric parameters may lead to nonlinear and remarkable amplification of mechanical properties [18–20]. Li et al. [21] brought out a generalized mechanical model to analyze the equivalent stiffness and failure mechanism of the sutural composites under different loading cases. He pointed out that triangular shape possesses the highest stiffness compared to trapezoidal, rectangular and anti-trapezoidal waveforms in both tension and shear. Gao et al. [22, 23] studied the sutural wavy tessellation in biological tissues and demonstrated the high enhancement of sutural interface on strength, toughness and auxeticity. Owing to the changes of the loading transmission paths, the stiffness and toughness can be anisotropically improved by changing the sutural angles. Furthermore, the mechanical models were analyzed and demonstrated by 3D printing experiments. Liu et al. [24] studied the failure mechanism of sutural composites. Triangular interface helped the composites understand much more stretching and shear loading. The crack propagation paths could be controlled by adjusting the suture interface parameters. Yu et al. [25] developed an analytical model to investigate the damping properties of bio-inspired composites with sutural interface. These work addressed the influence of sutural interfaces on the mechanical behavior of composite structures under quasi-static loading cases. Appropriately designed geometry of suture interfaces effectively utilizes the natural materials to achieve high mechanical properties and complex functions.

In natural composites, tissue staggered materials often perform more smart behavior. They can respond to external stimulus [26–28]. Natural composites can match their mechanical properties to the external stimulus to achieve higher protection. When impact with high rate or large strain is loaded upon the bionic composites, remarkable self-stiffening behavior can be resulted in order to protect biological organism [29]. Jia et al. [30] pointed out that appropriate stiffness ratio of soft materials and hard materials in biomimetic composites acts critical role in the capacities of impact resistance. The soft components help diminish dislocation motion and dissipate impact energy, while the stiff components hinder the propagation of the external stimulus. Kwonhwan et al. [31] pointed out appropriate volume ratio of soft and rigid material can lead to high resistance to impact in the nacre-like composites. To achieve better impact-resist capacities under various loading cases, artificial suspensions or gel materials offer an excellent solution for the self-hardening behavior. Among them, shear stiffening gel (SSG) has been widely adopted in biomimetic engineering materials, whose storage modulus can be sharply increased when strain rate is beyond a critical point [32]. Once the shear loading was removed, SSG returns to soft plastic state. It was expected in engineering application that this structure material held high elastic modulus to resist deformation under loading cases and high viscosity to dissipate residual kinetic energy under unloading cases. Large numbers of researches have been conducted to investigate the engineering application of SSG [33, 34]. It should be important to have an insight into the influence of SSG in sutural composites.

In this work, sutural composites were designed and fabricated via a 3D-printing method. A novel smart material, SSG, was adopted as interfacial material. The rheological tests and compressive tests with constant velocity indicated remarkable rate-dependent characteristics towards various external mechanical stimulus. Drop weight machine was adopted to investigate their capacities to resist impact with low velocity. The tests were conducted with fixed boundary and free boundary to evaluate the damping characteristics, which demonstrated the promising protection capacity of sutural composite. Furthermore, a finite element simulation was performed to analyze the experimental results and the stress evolution inside of the composites. Our study pointed out an effective method to improve the capacities of impact resistance and energy dissipation of the universal bionic composites.

Experiments section

Materials

To prepare the SSG, the boric acid (Sinopharm Chemical Reagent Co. Ltd., Shanghai, China) and hydroxyl silicone oil (500 mm2/s, AR degree, Jining Huakai Resin Co. Ltd.) were mixed at the mass ratio of 1:15 and heated at 180 °C for two hours (Fig. 1a). During the heating, the suspension system formed cross-linking and viscous paste. Then, 15 μl caprylic acid was poured into every 100 g paste. After another hour of heating, the SSG was obtained (Fig. 1b).

The preparation and fabrication procedures of sutural composites are shown in Fig. 1c–e. The sutural skin facesheets were printed using polylactic acid (PLA) by a 3D-printer (Creator 3, Flashforge Co., China). Skin facesheets and SSG were pressed into a cubic steel mold to get the sutural composites (Fig. 1e). The sizes of skin facesheets are illustrated in Fig. 2. The thickness of sutural composites, h, varied from 16, 18 to 20 mm. The thickness of skin facesheets, h_2, was 5.4 mm. The height of teeth, h_3, was set as 9.6 mm. The test specimens were categorized according to the vertex angle of teeth (θ in Fig. 2). According to previous researches [24], sutural composites with 30°, 45° and 60° showed remarkable enhancement on mechanical properties in quasi-static tension tests. Here, the same angles were adopted. The specimen with 180° teeth vertex angle was staggered composites without sutural interface. The areal density of 180° specimen was assured to be the same as that of sutural composites by adjusting the thickness of skin facesheets, h_1, to be 7.5 mm. The length and width of the skin facesheets, a and b, were 100 and 114 mm, respectively.

Characterization

The rheological properties of SSG were tested by commercial rheometer (Physica MCR 302, Anton Paar Co., Austria). Parallel plate testing model was adopted. The shear amplitude was set at 0.1%, and the shear frequency increased from 0.1 to 100 Hz logarithmically. The sample was molded into a columned structure with 1 mm in height and 20 mm in diameter, respectively. The creep-recovery behavior and strain-dependent behavior were also tested.

The compressive mechanical behavior of the sutural composites was tested by universal testing machine (Fig. 3a) (MTS criterion 43, MTS System Co., America). The compressive speeds were set as 0.01, 0.05, and 0.10 mm/s, respectively.

The dynamic mechanical behavior of sutural composites was tested by drop tower testing machine (Fig. 3b) (Mode ZCJ1302-A, MTS Industrial Systems (China) Co., LTD, China). The tested specimen was constrained by steel restraint devices in Fig. 3c–d. The hammer was 280 g in weight. The hammer head was hemispheric with 25 mm in diameter. The change of impact velocity was monitored by another piezoelectric acceleration sensor (Fig. 3c). Another acceleration sensor was adopted to record the motion of the bottom skin facesheets. Then, the acceleration sensor was replaced by a dynamic force sensor to record the transmission force. All sensor data were gathered synchronously by a digital acquisition system, including a charge amplifier (Mode YE5853, Jiangsu Sinocera Piezotronics, INC., China) and an oscilloscope (Mode DPO2012B, Tektronix INC., USA). The sampling rate was set as 100 kHz.

Figure 1 The illustration of the preparation of SSG and skin facesheets.
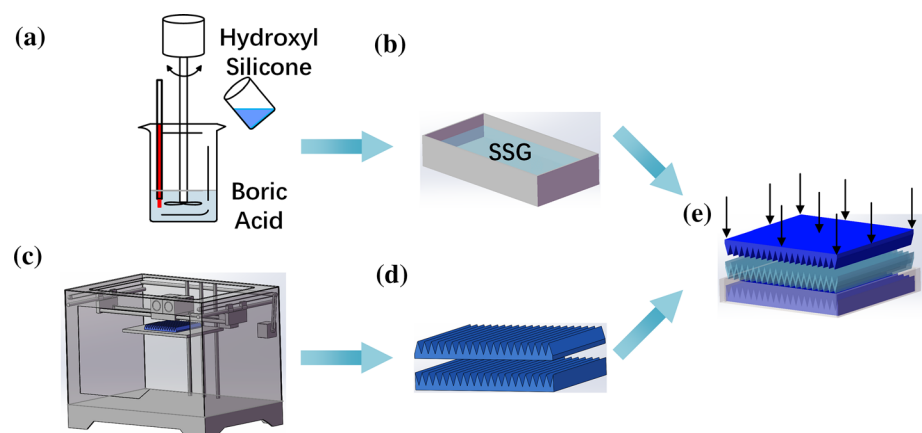
Figure 2 The dimension of sutural facesheets.
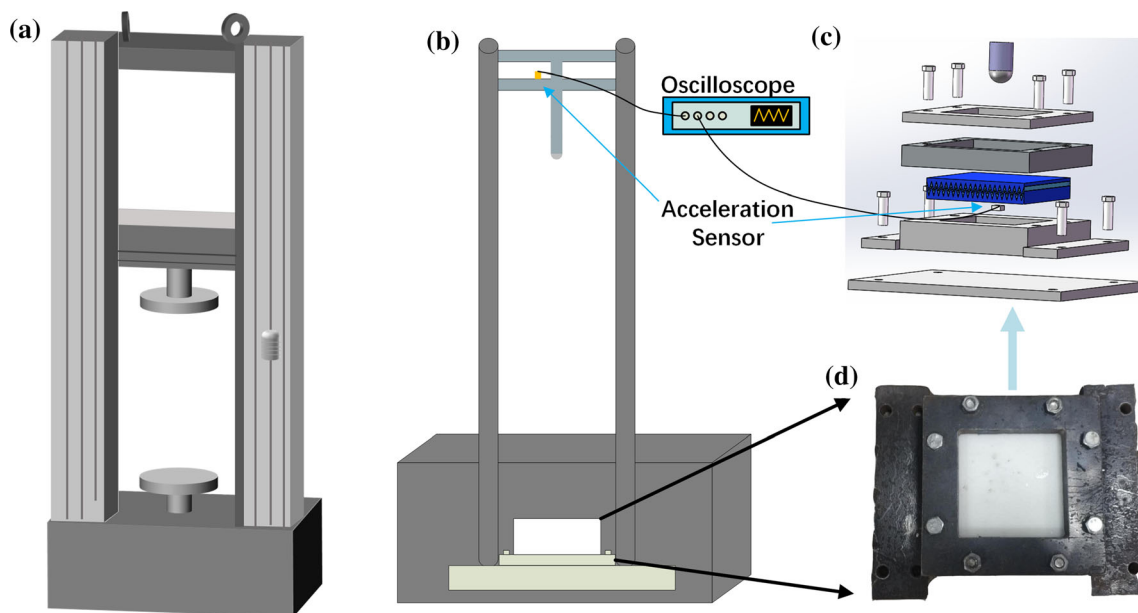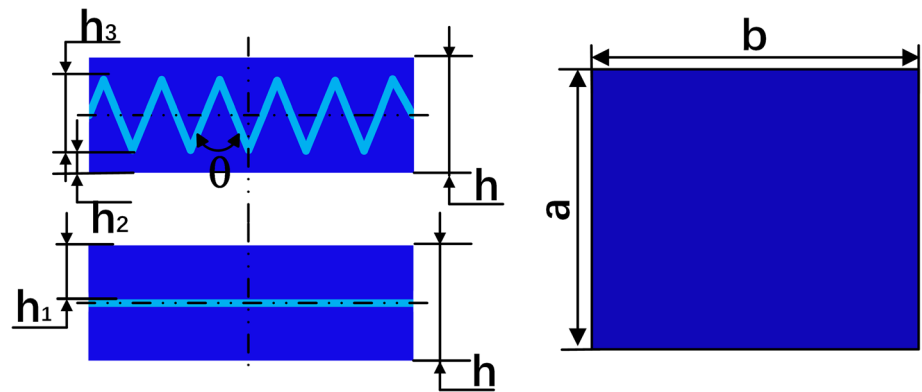
Figure 3 The MTS (**a**) and drop tower testing machine (**b**). **c**–**d** The constraint of specimen in drop tower tests.

Experiment results and discussion

Rheological properties of SSG

Figure 4a shows the rate-dependent behavior of SSG. The storage modulus of SSG was 0.76 kPa at 0.1 Hz. With the shear frequency increasing to 100 Hz, the storage modulus shifted to 282 kPa. However, the loss modulus increased with the shear frequency increasing to 2 Hz and then decreased. The damping factor was the ratio of loss modulus to storage modulus. It was usually adopted to indicate the solid characteristic of SSG. With the testing frequency increased to 100 Hz, damping factor decreased from 17.61 to 0.03, which indicated the SSG transformed from soft gel state to stiff rubbery state. To ensure the time effect of the rate-dependent behavior, creep and recovery tests were conducted and are shown in Fig. 4c. Constant shear stress was set at 50, 500 and 5 kPa. Shear stress was maintained for 30 s and then removed. The creep compliance showed remarkable dependence on external stress. The maximum creep strains were 2.97%, 20.66% and 136.8% when the shear stress was 50, 500 and 5 kPa, respectively. The shear modulus increased 1.68 to 3.67 kPa. However, the stiffening effect could not be held after the shear stress removed. The recovery behavior under 50 Pa was negligible. SSG showed typical plastic characteristic. With the increase in shear stress, instantaneous recovery strain became obvious. It came to be 21.9% when the external stress came to 5 kPa. Rate-dependent behavior was eliminated soon after the stress was removed, which demonstrated the reversible and swift translation of SSG between gel state
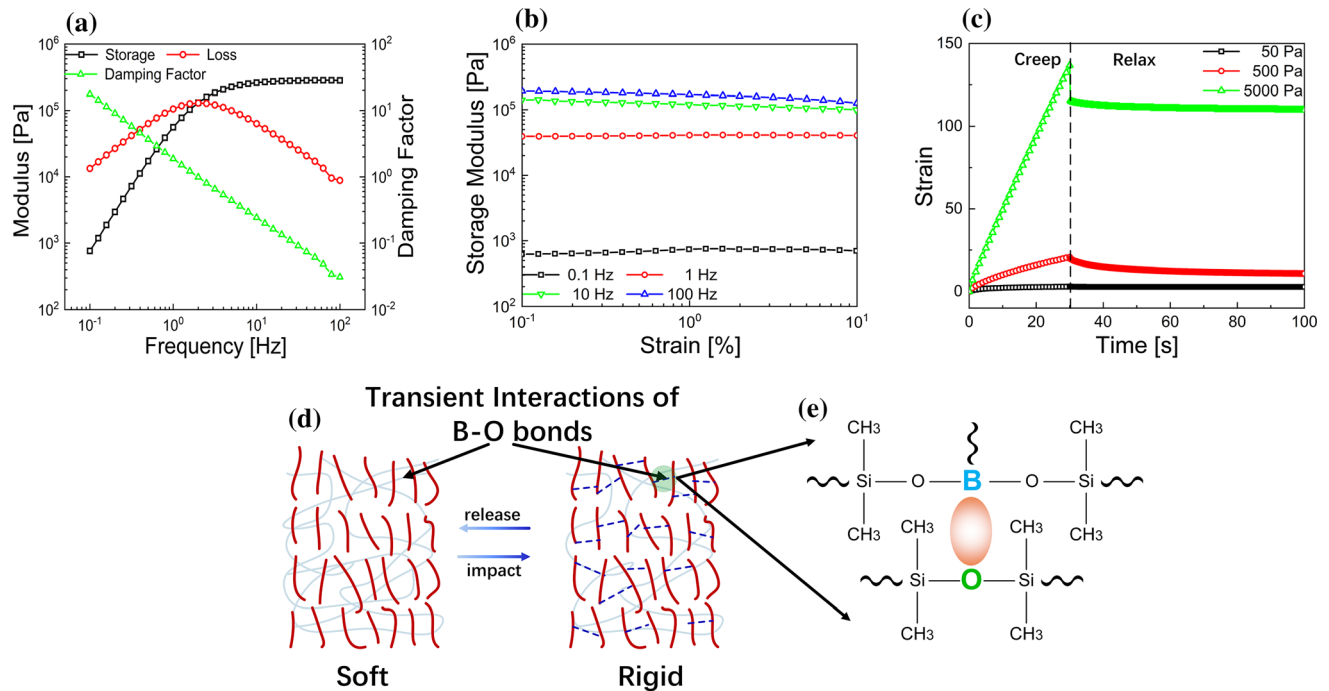
Figure 4 **a** Storage modulus and loss modulus of SSG under different shear frequencies. **b** Strain-dependent behavior of SSG under different shear frequencies. **c** Creep and recovery behavior of SSG under different shear stress. **d**–**e**) The shear stiffening mechanism.

and rubbery state. The influence of strain is shown in Fig. 4b. SSG could hold linear mechanical properties under large deformation, which would help the composites keep stable mechanical responses under external stimulus.

The shear stiffening behavior is illustrated in Fig. 4d-e. Without external stimulus, SSG was soft and deformable. Once shear stimulus was loaded, the shear stiffening characteristic led to local hardening progress of SSG. As illustrated in Fig. 4d, hardenability was positively related to strain rate. The rate-dependent behavior should be owed to the weak physical "B-O" bonds. This cross-bonds were transient and reversible. Stimulus with high rate did not permit enough relaxation time for B-O bonds. Polymer chains were hindered and heavy agglomerations were generated. Then, shear stiffening behavior was observed. Once the loading was removed, B-O bonds relaxed from each other and the impediment of agglomerations disappeared. SSG returned to soft state.
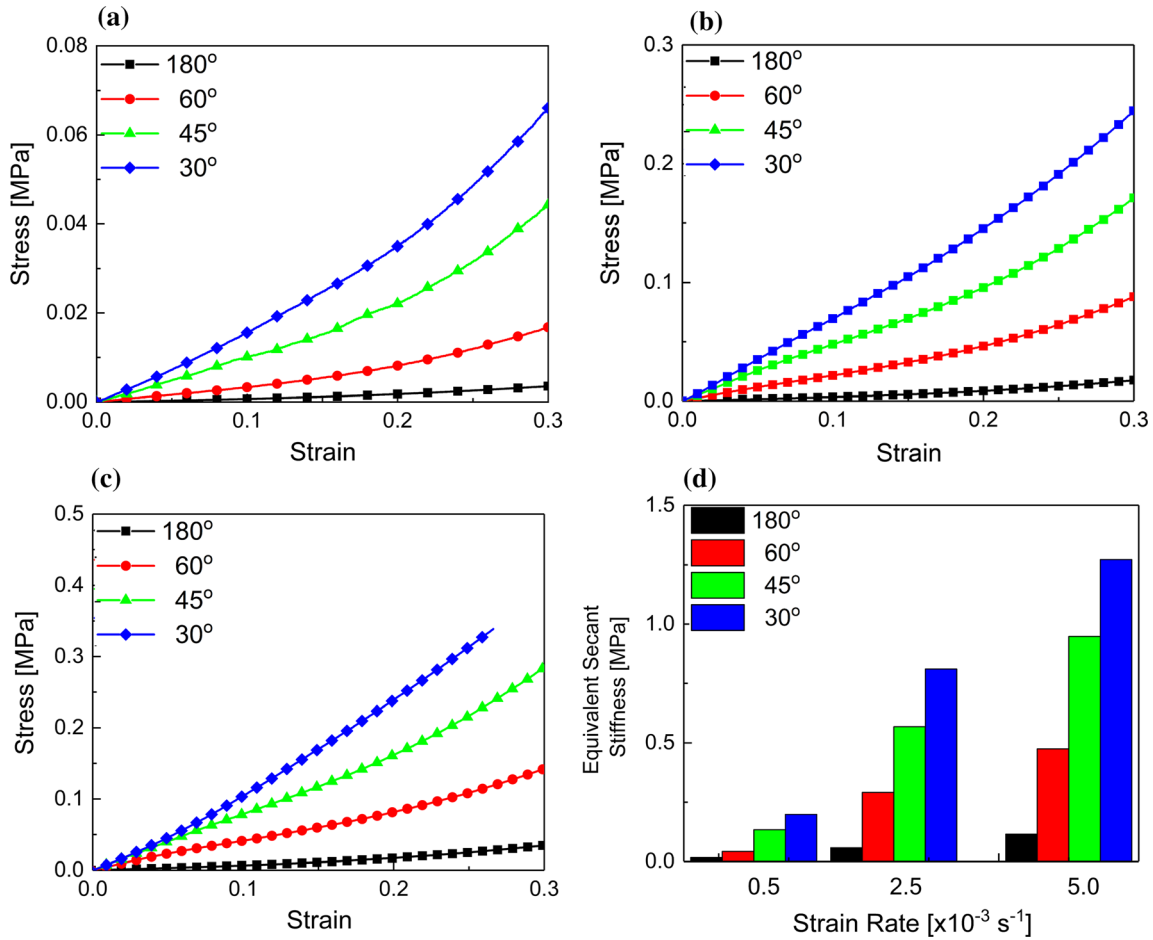
Compressive tests of the sutural composites

Compressive tests of the sutural composites under different compressive velocities were carried out. Engineering strain and stress are shown in Fig. 5a.

The compressive stress of the 180° sutural composite was 3.88 kPa when the compressive strain came to 0.3. As for the sutural composites with the teeth vertex angles in 60°, 45°, and 30°, the compressive stresses under the same compressive strain reached 16.62, 40.07, and 59.60 kPa, respectively. The enhancement of the suture interface on the mechanical properties was obvious. The inclinations of tooth surface would influence the mechanism of stress transmission. Here, a plane strain model was established to illustrate this enhancement. The thickness of SSG was h_0. λ and h were the wavelength and amplitude of the interfacial geometry (Fig. 6a). The model was subjected to a far-field stress, σ_y. Representative volume elements is shown in Fig. 6b. τ_n and τ_t were the normal stress and shear stress on the sutural teeth under local coordinate system. The inclination angle was $\frac{\theta}{2}$. Based on the plane strain model (Fig. 6b) of sutural angles, a force equilibrium equation could be brought out:

$$\tau_t(x)\cot\frac{\theta}{2}dx + \tau_n(x)dx = [\sigma_y(x) + d\sigma][x + dx] - \sigma_y(x)x$$

(1)

where $\tau_n = \tau_t \tan\frac{\theta}{2}$. Then, it could be obtained as

Figure 5 The mechanical behavior of sutural structures under compressing loading with the speed **a** 0.01 mm/s, **b** 0.05 mm/s, and **c** 0.10 mm/s. **d** The stiffness of the sutural composites under different compress rates.

$$\begin{cases} \tau_t = \sigma_y \sin\dfrac{\theta}{2}\cos\dfrac{\theta}{2} \\[2mm] \tau_n = \sigma_y \sin^2\dfrac{\theta}{2} \end{cases} \quad (2)$$

Considering the continuous boundary condition across the interface of SSG and facesheets, it could be obtained as

$$\begin{cases} \tau_{1t} = \gamma_t \\ \tau_{1n} = \tau_n \end{cases} \quad (3)$$

where τ_{1t}, τ_{1n} indicate the shear stresses and normal stresses of the SSG. The mechanical behavior of the soft SSG could be described by constitutive equation: $\tau_t = G_1\gamma_t$ and $\tau_n = E_1\gamma_n$, where the G_1 and E_1 indicate the shear modulus and elastic modulus of the SSG, and γ_t and γ_n indicated the shear strain and normal strain of the SSG. Considering SSG could be regarded as an incompressible, $E_1 = 2G(1 + v) = 3G_1$. v is the

Poisson's ratio of SSG. When the sandwich is subjected to a uniform normal external traction σ_y, an energy equilibrium equation could be brought out

$$W = \int_V \frac{\sigma_y \cdot \sigma_y}{E_y} dV = \int_{V_1} \varepsilon_1 \cdot \sigma_1 dV_1 + \int_{V_2} \varepsilon_2 \cdot \sigma_2 dV_2 \quad (4)$$

where E_y is the equivalent stiffness under plane stress model, W is the external energy. Under the assumption that the stress and strain are evenly distributed in the gap between the sandwich interfaces, the deformation energy could be solved:

$$\begin{cases} \displaystyle\int_{V_1} \varepsilon_1 \cdot \sigma_1 dV_1 = (1-f)h\lambda\sigma_y\sigma_y\left(\dfrac{\sin^4\frac{\theta}{2}}{E_1/(1-v^2)} + \dfrac{\sin^2\frac{\theta}{2}\cos^2\frac{\theta}{2}}{G_1}\right) \\[4mm] \displaystyle\int_{V_2} \varepsilon_2 \cdot \sigma_2 dV_2 = \dfrac{fh\lambda\sigma_y\sigma_y}{E_2} \end{cases} \quad (5)$$

where the E_2 indicates the elastic modulus of the

Figure 6 Illustration of the theory model (**a–b**) and the results (**c**).
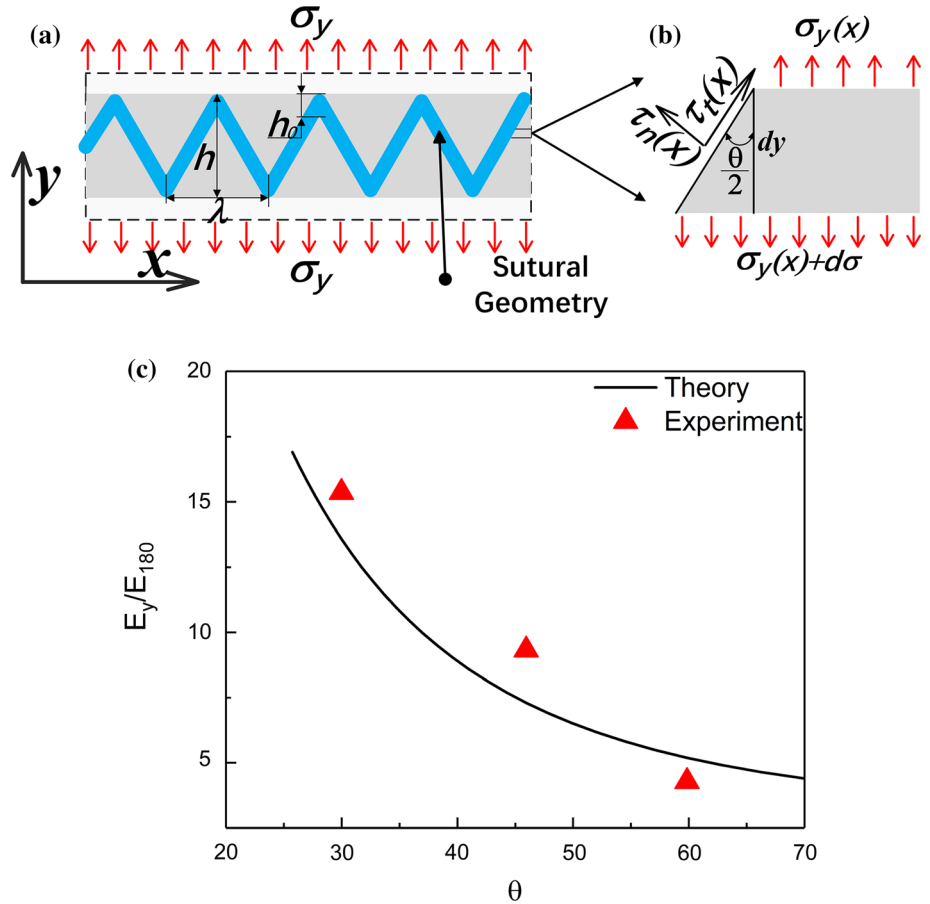
rigid teeth, f indicates the volume ratio of SSG in sutural geometry, $f = 1 - \frac{h_0}{h}$. The equivalent compressive modulus could be expressed as

$$E_y = \frac{1}{(1-f)\left(\frac{\sin^4\frac{\theta}{2}}{E_1/(1-v^2)} + \frac{\sin^2\frac{\theta}{2}\cos^2\frac{\theta}{2}}{G_1}\right) + \frac{f}{E_2}} \quad (6)$$

Based on this model, the equivalent compressive modulus ratio could be obtained and the results are shown in Fig. 6c. It matched well the compressive results. Therefore, sutural composites performed much higher equivalent stiffness (Table 1).

Meanwhile, the loading rate effect on the compression deformation was investigated (Fig. 5b–d). The peak force for the 180° staggered composite is 3.88 kPa at 0.01 mm/s and 34.62 kPa at 0.10 mm/s, respectively. As for the sutural composites, the peak force increased from 16.62, 40.07, 59.60 to 142.52, 284.59 and 338.16 kPa, respectively, with loading rates increasing from 0.01 to 0.10 mm/s. The magnification of the equivalent secant stiffness of the sutural structure was magnified for about 1113%,

708%, and 691% with sutural vertex angles in 60°, 45°, and 30°, respectively. The equivalent secant stiffness is summarized in Fig. 5d. It could be found that sutural composites achieved higher equivalent structural stiffness and more typical rate-dependent performance.

Low-velocity impact tests of sutural composites

The impact-resist capacity of the sutural structure was investigated by drop weight experiment. As illustrated in Fig. 7a, hardenability was positively related to strain rate. Shear strain rate near impact zone was much higher than that away from the impact zone in a continuous beam. SSG could perform remarkable different hardenability under

Table 1 Parameters in theory model

h_0 (mm)	h (mm)	E_1 (MPa)	E_2 (MPa)	v
1	9.6	0.01	296	0.49

impact. To evaluate the protective capacity of the composite structures, an acceleration sensor was fixed upon the bottom face of the sutural composite to record their motion data. Figure 7b shows the acceleration results of drop weight in the impact duration. The thickness of interfacial SSG was 1 mm. The peak values were 3.06, 3.02, 2.90 and 2.44 km/s^2 corresponding to the sutural composites with sutural angles of 30°, 45°, 60° and 180°. Under the same impact energy, the peak acceleration of sutural composites was much higher than the conventional 180° sutural composite. Meanwhile, the impact duration increased from 1.70 ms to 1.96 ms. To be more obvious, force–displacement curves are shown in Fig. 7c. Under the same impact loading case, contact force of the 30° sutural composite was much higher and the deformation was smaller than that of 180° sutural composite. When the loading progress finished, the deformations of the sutural composites were 1.33, 1.40, 1.53 and 1.65 mm with respective the sutural angles 30°, 45°, 60° and 180°. Meanwhile, the peak values of the contact force achieved 860, 837 797 and 665 N, respectively. Compared to the sutural composites without interfacial geometry, the contact stiffness was remarkably improved. Due to the

compression and relaxation of the interfacial SSG, the force–displacement curves were not smooth. Stiffness is presented in Fig. 7d. The stiffness of 30°, 45°, 60°, 180° sutural composites was 0.585, 0.540, 0.477 and 0.393 kN/mm, respectively. Sutural interface helped achieve an improvement of 48.8% in the stiffness.

To evaluate the protective capacity of sutural composites, the motion of the bottom facesheets was recorded by another acceleration sensor. Upon the drop weight touched the top facesheets, interfacial SSG endured squeezing force and transferred the loading to the bottom facesheets, which led the first rising in the acceleration. With the increase in deformation of bottom facesheets, elastic force from the face sheet came to exceed the squeezing force from interfacial SSG. Then, the acceleration came to decrease. When the bottom face sheet achieved its maximum deformation, the acceleration reached its peak values and the loading progress finished. Composites began to recover to initial state. Acceleration decreased to zero. Generally, the top face sheets endured impact, and the bottom face sheet was protected with the armor. It was expected that the deformation of the bottom facesheet was small. The peak values of bottom acceleration of sutural
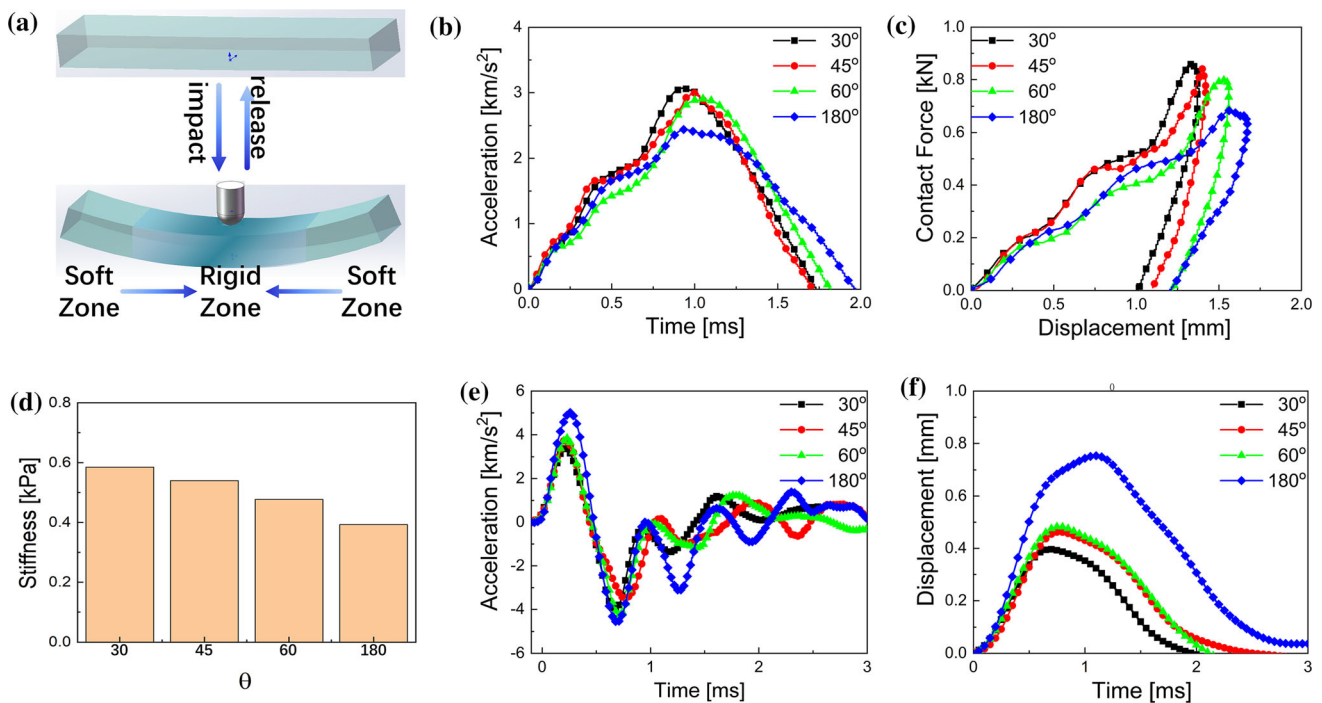
Figure 7 **a** Illustration of shear stiffening effect under impact loading case. **b** The acceleration data of drop weight with different sutural interface under the drop height of 0.2 m and **c** the contact force versus displacement curves. **d** The equivalent stiffness of sutural composites in the impact duration. **e** The acceleration of the bottom face sheet and **f** the deformation.

composite were 3.38, 3.74 and 3.84 km/s^2 with respective angles 30°, 45° and 60° (Fig. 7e). Compared to the 180° sutural composite, they achieved reduction of 33%, 25% and 24%. To be more obvious, the deformation was calculated and is shown in Fig. 7f. The presence of sutural interface effectively suppressed the deformation. The deformation reached 0.39, 0.46 and 0.48 mm as the sutural angles were 30°, 45° and 60°. However, the deformation of 180° sutural composite was 0.79 mm. Sutural interfaces showed remarkable enhancement in protective capacity compared to conventional structures.

Figure 8a shows the acceleration data of the drop weight test for sutural structure with 30°. With the increase in drop height, the impact duration was reduced from 1.74 to 1.52 ms. However, in the results of the conventional, impact duration held nearly constant around 1.78 ms. Meanwhile, the peak values of the acceleration in the same drop height also showed remarkable increase. The peak values of sutural composite were 3.066, 4.450, 5.591 and 6.749 km/s^2 when the drop heights were 0.2, 0.4, 0.6 and 0.8 m, respectively. Compared to the acceleration of 180° sutural composite, the increases were 19.4%, 16.5%, 17.8%, and 19.7%, respectively. Figure 8b,e

illustrates the force–displacement curves of the 30° sutural composite and 180° sutural composite. The inclination of the curves in rising stages could be considered the stiffness of composites. Due to the typical rate-dependent characteristic of SSG, the stiffness of sutural composites dropped fast after the loading progress finished. SSG returned from rigid rubbery state to soft gel state, which led to the large residual deformation. When the drop heights were 0.2, 0.4, 0.6, and 0.8 m, the stiffness of sutural composite were 0.585, 0.705, 0.748 and 0.806 kN/mm. The increase in drop height led to an increase of 36.4% in stiffness. Meanwhile, when the drop height increased to 0.4 m, the stiffness of 180° sutural composite nearly held constant at 0.54 kN/mm. Sutural interface changed the deformation mechanism of SSG and enlarged the local strain, which led to the enhancement in stiffness and remarkable rate-dependent behavior.

The energy dissipation ratio could be calculated by the enveloped area by the force–displacement curves. Owing to the typical rate-dependent behavior of SSG, large numbers of impact energy were dissipated by SSG via the phase transformation. However, sutural interface showed negative effect on the energy
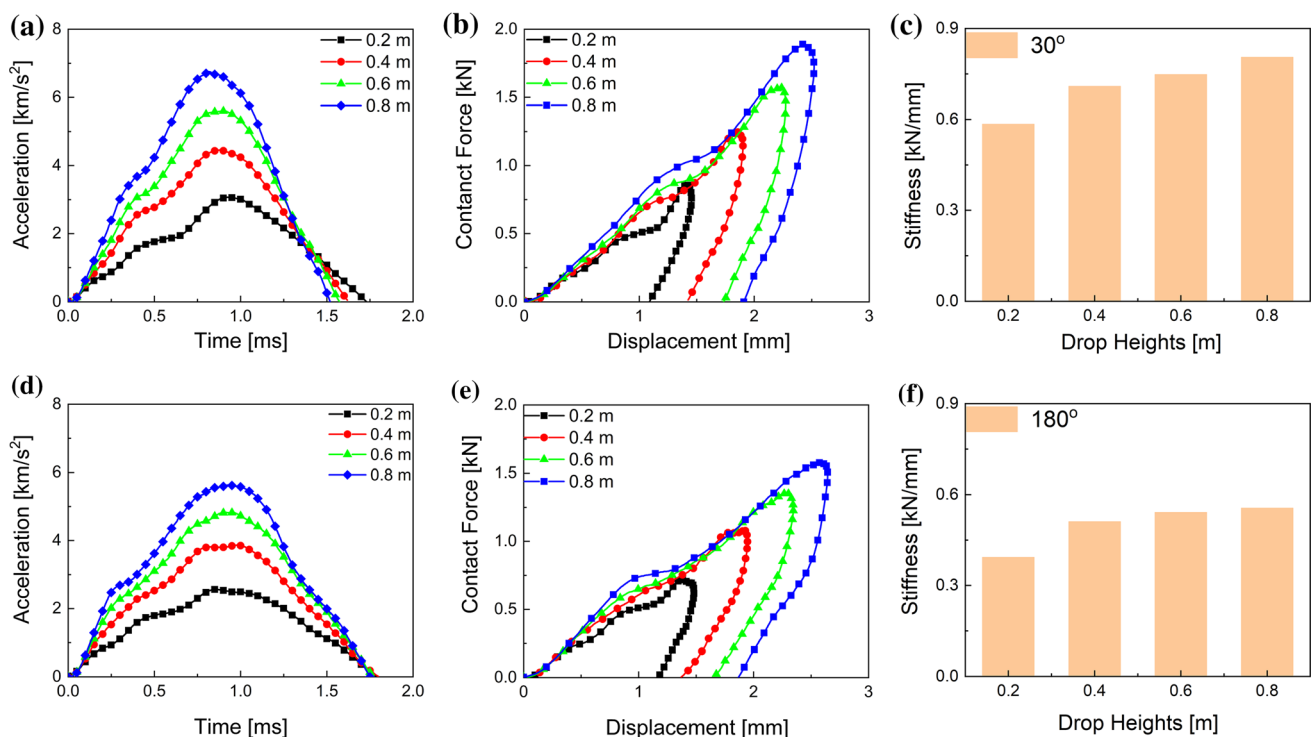

Figure 8 a The acceleration results, b contact force versus displacement and c stiffness of sutural composites with sutural angle of 30°. d–f) The results of 180° sutural composite.

dissipation under small drop height. When the drop height was 0.2 m, the dissipation ratios were 0.81, 0.80, 0.82 and 0.86 with respective sutural angles 30°, 45°, 60° and 180° (Fig. 9). With the increase in drop height, the dissipation ratio of 180° sutural composite decreased. Higher impact energy led to the shear stiffening behavior of SSG and composites came to be more rigid. The growth of solidity diminished the energy dissipation capacity. However, sutural composite with 30° showed stable energy dissipation capacity. It worked better under heavy impact stimulus compared to the 180° sutural composites.

Furthermore, the role of the thickness was investigated. The thickness of interfacial SSG varied from 1, 3 to 5 mm. The results of sutural composites with 30° are shown in Fig. 10. With the increase in thickness of interfacial SSG, the rising progress of acceleration was suppressed. When the thickness of SSG was 3 and 5 mm, the response of acceleration performed on a plateau period. The peak values were significantly reduced. Correspondingly, the plateau was observed in force–displacement curves. However, sutural composite with 1 mm showed more remarkable rate-dependent behavior. With the increase in drop height, impact duration was shortened in the specimen with 1 mm in thickness. The impact duration of the other two specimen held nearly constant.

To further investigate the protection capacity of the sutural composites, a dynamic force sensor was fixed upon the bottom facesheets instead of the acceleration sensor (Fig. 11a). Compared to the previous tests, the dynamic force sensor provided a fixed boundary at the center of the bottom facesheets. The
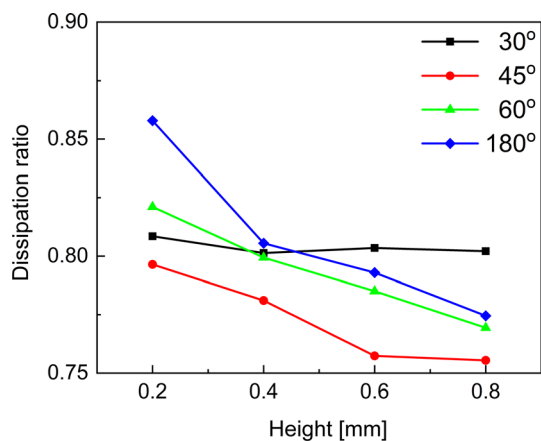
peak values of the contact force of the sutural composites were higher than those of the 180° sutural composite. Sutural composites with 30° and 45° held similar peak values at different drop heights (Fig. 11b–d). The peak acceleration of 60° sutural composite was much smaller. Small sutural angles helped hold high stiffness. However, support force showed different trends. With the strengthening of stiffness, support force also increased to some degree. Here, the transmissibility factor (TF) was defined as the ratio between contact force and support force. The relationship between TF and drop heights is illustrated in Fig. 12. The increase in drop height led to ascent of TF values, indicating that the more elastic part came to dominate the mechanical behavior. It should be noted that the TF value of sutural composite was always less than 1 regardless of impact height. The presence of sutural interface effectively suppressed the transmission of impact force. It would help reduce the impact force action and have a certain impact protection ability.

Numerical analysis on the impact behavior of sutural composite

To understand the influence of suture interface on the impact behavior of sutural composites, finite element analysis (FEA) was adopted to study the impact deformation of different specimens. As shown in Fig. 13a, four different models were established in ABAQUS according to actual sizes of the experimental sutural specimens. Drop hammer was simplified as a rigid cylinder with semi-sphere, and the mass was 280 g. The mechanical properties of the skin facesheets were as follows: density ρ = 800 kg/m^3, Young's modulus E = 1300 MPa, Poisson ratio υ = 0.38. The density of SSG was 1.01×10^3 kg/m^3, Poisson ratio υ = 0.49.

Here, Cowper–Symonds model was adopted to describe the rate-dependent behavior. Rheological properties of SSG were characterized by steady shear test via MCR302. In Cowper–Symonds model, the dynamic yield stress depended on the strain rate of SSG. The relationship of yield stress σ_y and effective plastic strain $\varepsilon_p^{\mathrm{eff}}$ could be expressed as follows:

$$\sigma_y = [1 + (\frac{\dot{\varepsilon}}{C})^{\frac{1}{q}}][A + B(\varepsilon_p^{\mathrm{eff}})^n] \tag{7}$$

where A is the initial effective yield stress, B and n represent the plastic hardening parameter and plastic

Figure 9 The energy dissipation ratio of different sutural composites.
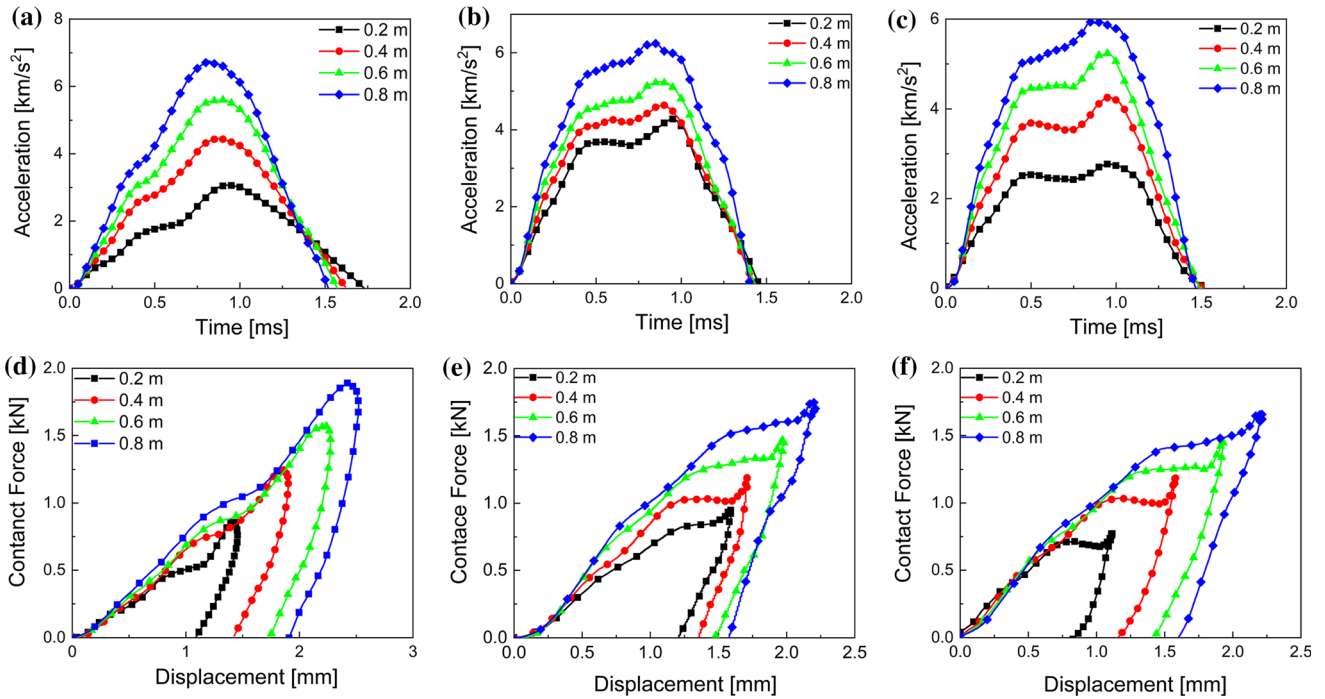
Figure 10 The drop weight tests of sutural composite with a different thickness of interfacial SSG, **a,b** 1 mm, **c,d** 3 mm and **e,f** 5 mm. The sutural angle was 30°.

Figure 11 a Illustration of force method of drop weight tests. And the result of sutural composites under different drop heights **b** 0.2 m, **c** 0.4 m and **d** 0.6 m. The solid lines were the results of contact forces, and the dash lines illustrated the support forces.
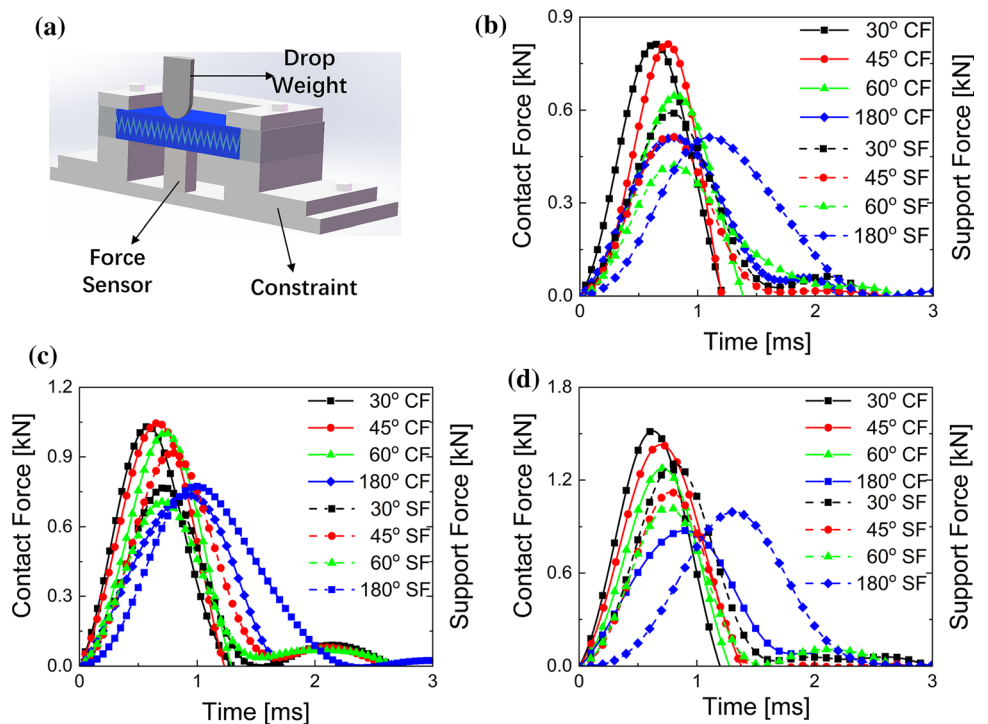

strain index. C and q were the rate-dependent parameters. First, the parameters A, B and n were obtained according to the results of quasi-static testing results. The shear rate was kept at 0.01 s⁻¹. It was obvious that the Cowper–Symonds model could well fit the experiment data (Fig. 13b,c). Thus, the Eq. (7) could be expressed as:

$$\tau_y = \left[1 + \left(\frac{\dot{\varepsilon}}{C}\right)^{\frac{1}{q}}\right]\left[227.45 + 69.864\left(\varepsilon_p^{\mathrm{eff}}\right)^{0.067}\right] \quad (8)$$

$$\ln\left[\frac{\tau}{227.45 + 69.864(\varepsilon_p^{\mathrm{eff}})^{0.067}} - 1\right] = \frac{\ln\dot{\gamma}}{q} - \frac{\ln C}{q} \quad (9)$$

To obtain good fitting relationship between σ_y and $\dot{\varepsilon}$, Eq. (8) could be transformed into:
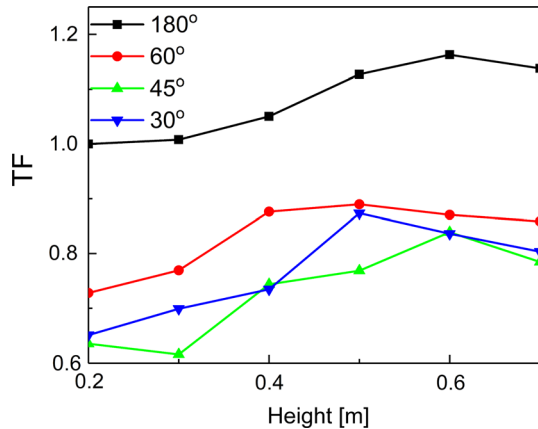
Figure 12 The force transmissibility ratio of sutural composite under different drop heights.

The effective yield shear stress was obtained via steady shear tests with different shear rates (0.1, 0.5, 1, 2, and 3 s^{-1}). The linear fitting results are shown in Fig. 13c. The slope of the fitting line was $1/q$ and the intercept represented $-\ln C/q$. According to the fitting results, $q = 1.167$, $C = 6.386 \times 10^{-3}$. The constitutive equation of SSG under Cowper–Symonds model could be expressed as follows:

$$\tau_y = \left[1 + \left(\frac{\dot{\varepsilon}}{6.386 \times 10^{-3}}\right)^{\frac{1}{1.167}}\right]\left[227.45 + 69.864\left(\varepsilon_p^{\mathrm{eff}}\right)^{0.067}\right] \quad (10)$$

Stress–strain curves are plotted in Fig. 13d according to the Eq. (10) and experiment data. With different shear rates, the model could fit the experiment results well. Considering that the SSG could be regarded as incompressible material, $E = 2G(1 +$
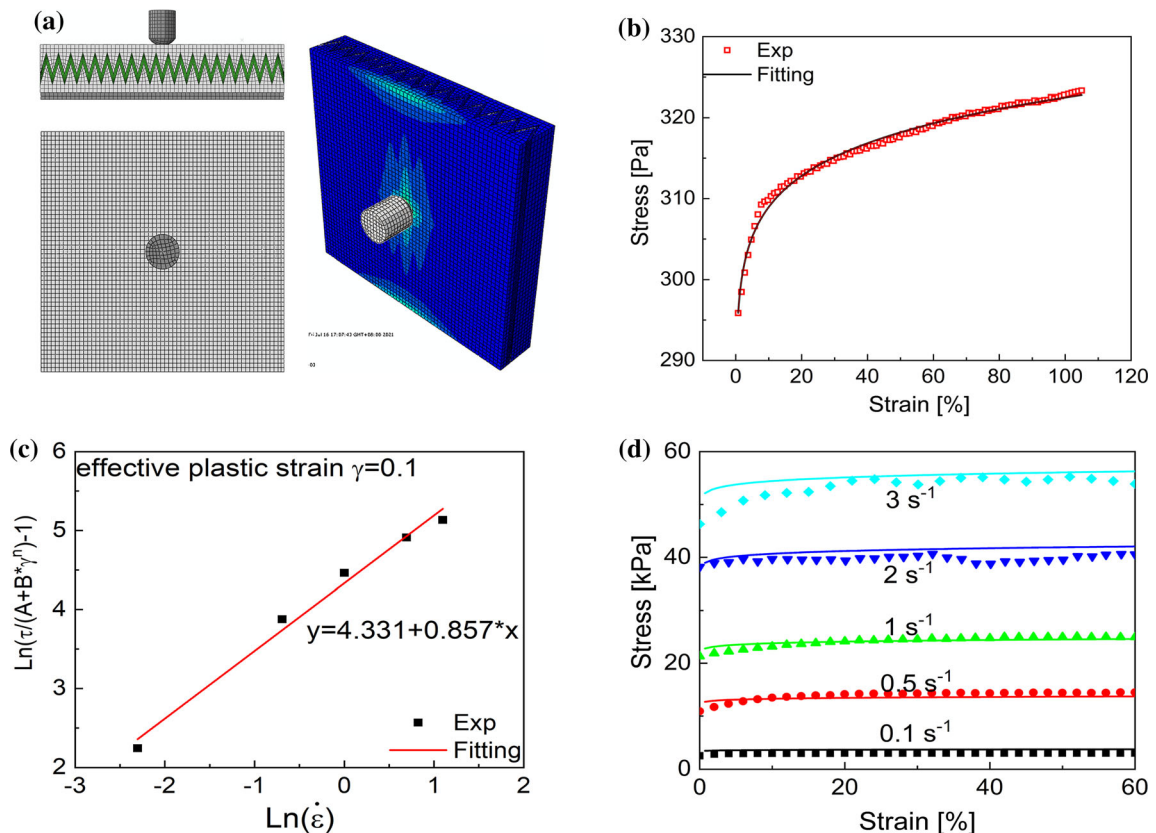
Figure 13 **a** The numerical model and their mesh method. **b, c** The fitting method of Cowper–Symonds model and **d** the validation results for this model. The solid lines were experiment data, and the dash lines were numerical data.
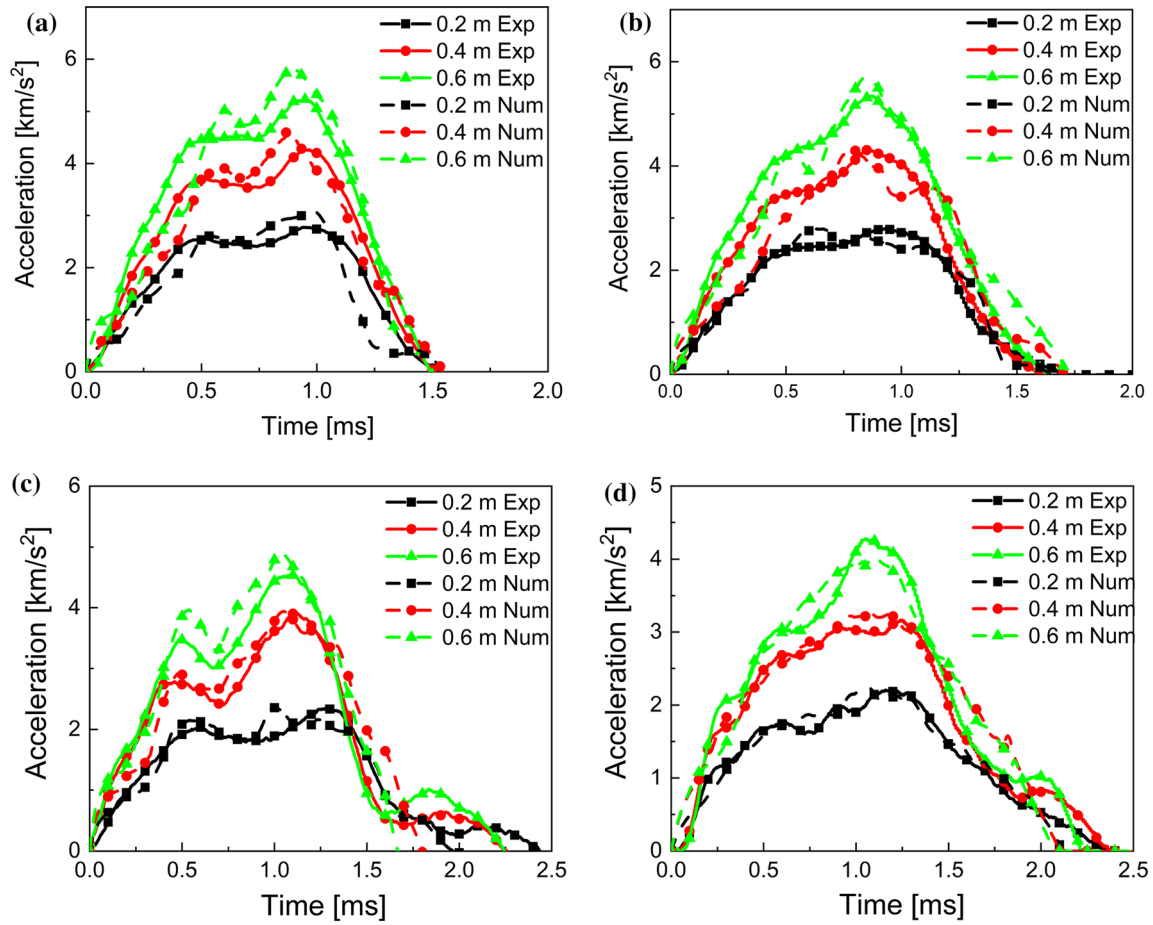
Figure 14 The comparison of experimental data (solid line) and numerical data (dash line). **a** 30°. **b** 45°. **c** 60°. **d** 180°.
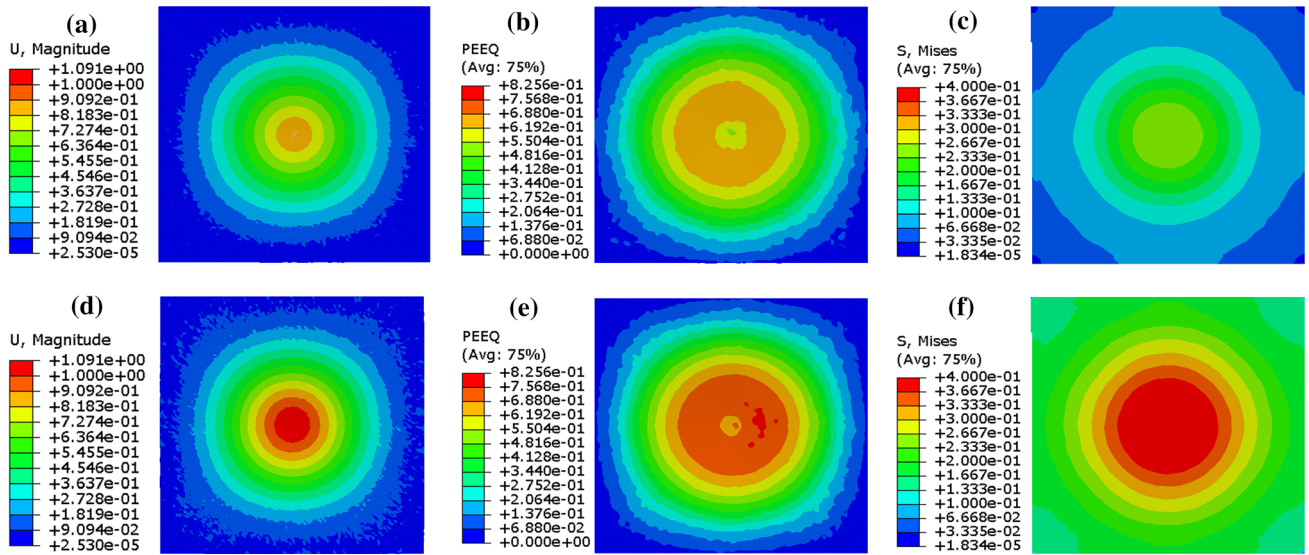
Figure 15 The deformation (**a**), equivalent plastic strain (PEEQ) (**b**) and von Mises stress (**c**) of 180° sutural composite with the drop height of 0.2 m. (**d**–**f**) The results under 0.6 m.

Figure 16 The distribution of LE on the bottom skin facesheets of sutural composites. **a** 30°, **b** 45°, **c** 60°, **d** 180°.
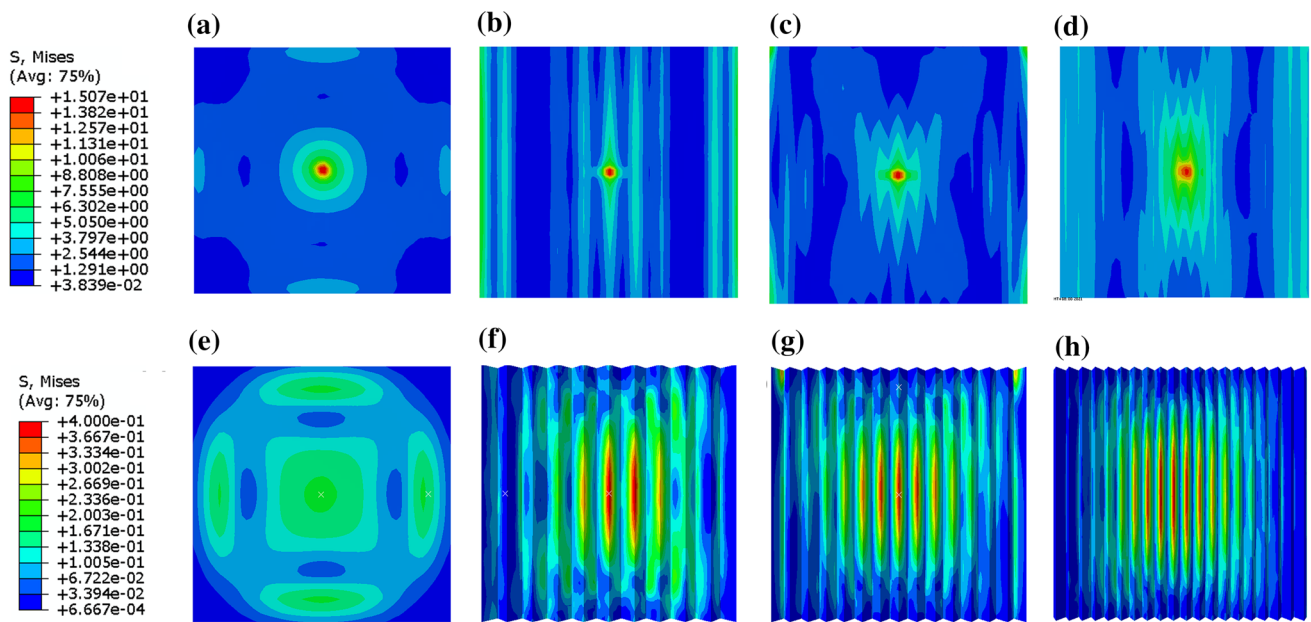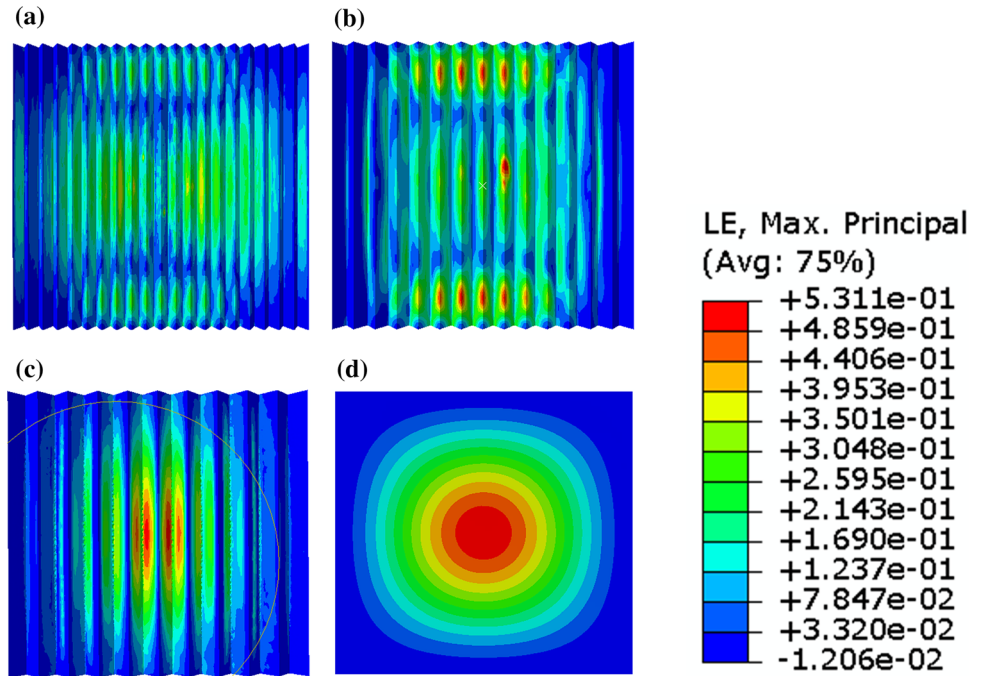
Figure 17 The comparison of von Mises stress contours among different suture structures. The stress distribution of top face sheets of 180° (**a**), 60° (**b**) 45° (**c**) 30° (**d**). **e**–**h** The stress distribution of bottom face sheets corresponding to that of the top face sheets.

$v) = 3G$. The final constitutive equation for SSG is as follows:

$$\sigma_y = \left[1 + \left(\frac{\dot{\varepsilon}}{6.386 \times 10^{-3}}\right)^{\frac{1}{1.167}}\right]\left[682.35 + 209.592\left(\varepsilon_p^{\text{eff}}\right)^{0.067}\right] \quad (11)$$

The initial Young's modulus of SSG was obtained according to the elastic scope in Fig. 4a and defined as 2.28 kPa. The structures were all meshed with C3D8R, 8-node linear brick, reduced integration element. Approximate mesh size of the sutural composites was set 0.5. The mesh around the suture angles would be refined to avoid the solution

divergence caused by large distortion. Acceleration of gravity was set along the z direction. The boundaries of face sheets were fixed. The initial velocity of the rigid ball was set according to the drop height. To demonstrate the goodness of the fitting results, the acceleration of drop harmer of different sutural structures is shown in Fig. 14.

The rate-dependent behavior of SSG is shown in Fig. 15. Generally, strain in a continuous beam was nearly linear about its coordinate. Figure 15a shows the deformation contour of interfacial SSG. Considering the impact stimulus was continuous forward loading, total strain could be divided into plastic strain and elastic strain. Deformation concentrated on the center of sutural composite, and the strain achieved its maximum values at the impact zone. However, owing to the hardenability of strain rate, the yield stress of SSG around the impact zone was largely improved. Plastic strain dominated around the impact zone and was eliminated at the center of impact zone. The elastic strain became the dominate form of deformation (Fig. 15b). The von Mises stress contour is shown in Fig. 15c. The stress did not show a declined behavior consistent with the plastic strain, which illustrated the self-hardening progress of SSG. With the increase in drop heights, equivalent plastic strain came to concentrate around the center of the interfacial SSG, and the maximum stress was distributed to a larger region (Fig. 15d–f). However, equivalent plastic strain at the center of the SSG still held constant, which indicated a typical shear stiffening behavior of SSG.

Furthermore, the role of suture teeth was investigated. Figure 16 illustrates the distribution of LE on the bottom skin facesheets at 1 ms. Owing to the presence of sutural geometry, deformation of bottom skin facesheets extends along the inclined interface instead of uniformly along the 180° plane. Large deformation was distributed at the edges of skin facesheets, which could help illustrate the result in Fig. 6f. With the increase in sutural angles, strain came to concentrate around the center of bottom skin facesheets. Impact energy was translated from top skin facesheets to bottom facesheets.

Figure 17 shows the distribution of von Mises stress on the top face sheet and bottom facesheet of different suture structures. The maximum stress of 60° top face sheet was smaller than that of 180° top face sheet. However, the stress was distributed to a larger scope with the presence of suture teeth, in which way the suture face sheets could provide higher contact stiffness. The distribution of stress on bottom face sheets is shown in Fig. 17e–h. Compared to the uniform distribution on 180° face sheet, the stress concentrated on the edges of the suture teeth and spread along the edge. With the decrease in suture teeth angles, the edges of the suture geometry undertook more stress. More serious stress concentration was observed at the edges of 30° suture structure. Heavy stress concentration might destroy the structures of suture geometry. However, the stress was reduced rapidly along the inclined suture planes. On the bottom of the suture angles, the stress was much smaller than that on the 180° bottom face sheet. The stress was heavily diminished during the propagation along the inclined suture planes. So, the TF was much smaller with the presence of suture geometry.

Conclusions

In this paper, biomimetic composites with suture interface were made by a 3D printer and the interfacial material was chosen as rate-dependent material, SSG. Compressive tests with constant speeds and low-velocity impact experiments were performed to evaluate the stiffness and impact protection properties. The following conclusions could be brought out:

The viscoelastic soft core in sutural composite showed high rate-dependent behavior. Its transient and mutable transformation from solid to plastic helps the sutural composite dissipate large energy. With the increase in drop heights, sutural composites with SSG showed more remarkable hardening behavior.

Sutural interface provided sutural composites with higher capacity to resist deformation and dissipate impact energy. The equivalent stiffness of sutural structure increased with the decrease in suture angles. Meanwhile, the deformation amplitude of the bottom face sheets was greatly decreased, and the impact energy could be dissipated in shorter time. The dynamic force sensor also showed that TF factors were also reduced owning to the suture geometry. These differences between the staggered composites with and without suture geometry came to more obvious when the impact energy increased. The composites were expected to be adopted as sutural materials to resist impact and vibration. It was hoped

to provide high structural stiffness and suppress residual kinetic energy.

The numerical analysis showed that the appropriate choice of the suture angles could make the deformation more uniform to enhance energy dissipation. Large contact area of the SSG was favorable for stress dispersion and the stress propagation along the triangle edges. Fine designed sutural geometry may lead to high suppression of impact stress.

Acknowledgements

References

[1] Malik IA, Barthelat F (2016) Toughening of thin ceramic plates using bioinspired surface patterns [J]. Int J Solids Struct 97–98:389–399

[2] Abo Sabah SH, Kueh ABH, Al-Fasih MY (2017) Comparative low-velocity impact behavior of bio-inspired and conventional sandwich composite beams [J]. Compos Sci Technol 149:64–74

[3] Malik IA, Barthelat F (2018) Bioinspired sutured materials for strength and toughness: Pullout mechanisms and geometric enrichments [J]. Int J Solids Struct 138:118–133

[4] Krollmann J, Schreyer T, Veidt M, Drechsler K (2019) Impact and post-impact properties of hybrid-matrix laminates based on carbon fiber-reinforced epoxy and elastomer subjected to low-velocity impacts [J]. Compos Struct 208:535–545

[5] Zhang P, Heyne MA, To AC (2015) Biomimetic staggered composites with highly enhanced energy dissipation: Modeling, 3D printing, and testing [J]. J Mech Phys Solids 83:285–300

[6] Katayama I (2021) Strength models of the terrestrial planets and implications for their lithospheric structure and evolution [J]. Prog Earth Planet Sci 8(1):1–17

[7] Lee N, Williams LN, Mun S, Rhee H, Prabhu R, Bhattarai KR, Horstemeyer MF (2017) Stress wave mitigation at suture interfaces [J]. Biomed Phys Eng Express 3(3):035025

[8] Rayneau-Kirkhope D, Mao Y, Rauch C (2018) Bioinspired hierarchical designs for stiff, strong interfaces between materials of differing stiffness [J]. Phys Rev Appl 10(3):034016

[9] Lyu Q, Zhang NH, Zhang CY, Wu JZ, Zhang YC (2020) Effect of adsorbate viscoelasticity on dynamical responses of laminated microcantilever resonators [J]. Compos Struct 250:10

[10] Meng L, Lan XQ, Zhao J, Wang ZM (2020) Equivalent models and mechanical properties of bio-inspired corrugated sandwich structures subjected to bending loads [J]. Compos Struct 244:10

[11] Li YN, Ortiz C, Boyce MC (2011) Stiffness and strength of suture joints in nature [J]. Phys Rev E 84(6):062904

[12] Alheit B, Bargmann S, Reddy BD (2020) Computationally modelling the mechanical behaviour of turtle shell sutures— A natural interlocking structure [J]. J Mech Behav Biomed 110:103973

[13] Liu ZQ, Zhang ZF, Ritchie RO (2020) Interfacial toughening effect of suture structures [J]. Acta Biomater 102:75–82

[14] Wu D, Zhao Z, Wang PD, Pei YM, Chen HS, Qi HJ, Fang DN (2020) Structured interfaces for improving the tensile strength and toughness of stiff/highly stretchable polymer hybrids [J]. Adv Mater Technol 5(11):11

[15] Wang WZ, Sun YP, Lu YY, Wang JP, Cao Y, Zhang C (2021) Tensile behavior of bio-inspired hierarchical suture joint with uniform fractal interlocking design [J]. J Mech Behav Biomed 113:12

[16] Lin E, Li Y, Ortiz C, Boyce MC (2014) 3D printed, bio-inspired prototypes and analytical models for structured suture interfaces with geometrically-tuned deformation and failure behavior [J]. J Mech Phys Solids 73:166–182

[17] Chen Z, Wu T, Nian G, Shan Y, Liang X, Jiang H, Qu S (2018) Ron Resch origami pattern inspired energy absorption structures [J]. J Appl Mech 86(1):011005

[18] Naleway SE, Porter MM, McKittrick J, Meyers MA (2015) Structural design elements in biological materials: application to bioinspiration [J]. Adv Mater 27(37):5455–5476

[19] Miroshnichenko K, Liu L, Tsukrov I, Li Y (2018) Mechanical model of suture joints with fibrous connective layer [J]. J Mech Phys Solids 111:490–502

[20] Cao Y, Wang W, Wang J, Zhang C (2019) Experimental and numerical study on tensile failure behavior of bionic suture joints [J]. J Mech Behav Biomed 92:40–49

[21] Li Y, Ortiz C, Boyce MC (2013) A generalized mechanical model for suture interfaces of arbitrary geometry [J]. J Mech Phys Solids 61(4):1144–1167

[22] Gao C, Hasseldine BPJ, Li L, Weaver JC, Li YN (2018) Amplifying strength, toughness, and auxeticity via wavy sutural tessellation in plant seedcoats [J]. Adv Mater 30(36):8

[23] Gao C, Li Y (2019) Mechanical model of bio-inspired composites with sutural tessellation [J]. J Mech Phys Solids 122:190–204

[24] Liu L, Li YN (2018) Failure mechanism transition of 3D-printed biomimetic sutures [J]. Eng Fract Mech 199:372–379

[25] Yu Z, Liu J, Wei X (2020) Achieving outstanding damping performance through bio-inspired sutural tessellations [J]. J Mech Phys Solids 142:104010

[26] Pogoda K, Chin L, Georges PC, Byfield FJ, Bucki R, Kim R, Weaver M, Wells RG, Marcinkiewicz C, Janmey PA (2014) Compression stiffening of brain and its effect on mechanosensing by glioma cells [J]. New J Phys 16:075002

[27] van Oosten AS, Vahabi M, Licup AJ, Sharma A, Galie PA, MacKintosh FC, Janmey PA (2016) Uncoupling shear and uniaxial elastic moduli of semiflexible biopolymer networks: compression-softening and stretch-stiffening [J]. Sci Rep 6:19270

[28] Engstrom TA, Pogoda K, Cruz K, Janmey PA, Schwarz JM (2019) Compression stiffening in biological tissues: On the possibility of classic elasticity origins [J]. Phys Rev E 99(5–1):052413

[29] Wu J, Yuan H, Li L, Fan K, Qian S, Li B (2018) Viscoelastic shear lag model to predict the micromechanical behavior of tendon under dynamic tensile loading [J]. J Theor Biol 437:202–213

[30] Jia Z, Wang L (2019) 3D printing of biomimetic composites with improved fracture toughness [J]. Acta Mater 173:61–73

[31] Ko K, Jin S, Lee SE, Hong J-W (2020) Impact resistance of nacre-like composites diversely patterned by 3D printing [J]. Compos Struct 238:111951

[32] Cross R (2012) Elastic and viscous properties of Silly Putty [J]. Am J Phys 80(10):870–875

[33] Liang J, Zhang XH (2015) Rheological properties of SP in shock transmission application [J]. J Mater Civil Eng 27(9):04014250

[34] Lin XG, Guo F, Du CB, Yu GJ (2018) The mechanical properties of a novel STMR damper based on magnetorheological silly putty [J]. Adv Mater Sci Eng 2018:1–15